Photochemical & Photobiological Sciences

PAPER

View Article Online
View Journal | View Issue

Cite this: *Photochem. Photobiol. Sci.*, 2016, **15**, 1282

# A Prussian blue/carbon dot nanocomposite as an efficient visible light active photocatalyst for C–H activation of amines†

Houcem Maaoui,[a,b] Pawan Kumar,[c,d] Anurag Kumar,[c,d] Guo-Hui Pan,[e] Radouane Chtourou,[f] Sabine Szunerits,[a] Rabah Boukherroub*[a] and Suman L. Jain*[c]

Received 15th June 2016,
Accepted 29th August 2016

DOI: 10.1039/c6pp00203j

www.rsc.org/pps

A Prussian blue/carbon dot (PB/CD) nanocomposite was synthesised and used as a visible-light active photocatalyst for the oxidative cyanation of tertiary amines to α-aminonitriles by using NaCN/acetic acid as a cyanide source and $H_2O_2$ as an oxidant. The developed photocatalyst afforded high yields of products after 8 h of visible light irradiation at room temperature. The catalyst was recycled and reused several times without any significant loss in its activity.

## 1. Introduction

Visible-light-driven photoredox catalysis is considered to be a promising strategy towards the development of a variety of chemical transformations in organic synthesis. These reactions use visible light, which is clean, abundant and renewable.[1] Of particular interest is the C–H activation of amines, because the resulting α-aminonitriles are highly important intermediates for the synthesis of bioactive natural products, unnatural α-amino acids or heterocyclic compounds.[2] The industrial synthesis of α-aminonitriles is achieved by the Strecker reaction between a carbonyl compound, an amine and a cyanide.[3] Similarly, a number of stoichiometric reagents which usually produce copious amounts of undesirable waste have been used for their synthesis. In the recent decades, catalytic methodologies using transition metal based catalysts such as $RuCl_3$,[4] $MnO_2$,[5] $Pd(OAc)_2$,[6] $V_2O_5$,[7] $FeCl_3$[8] and $[dpyCl_2Au^{III}]Cl$[9] have been developed for such a transformation. However, these catalytic processes commonly proceed at the expense of intense thermal energy and therefore are less desirable. Recently, molecular homogeneous photocatalysts based on Ir and Ru have been reported for this chemical transformation.[10] However, their high cost, toxicity and homogeneous nature are certain drawbacks, which make their utility limited towards practical applications. Consequently, heterogeneous photocatalysis is believed to be an interesting alternative to address the issues of non-recyclability of the homogeneous catalysts. Recently, our group reported the synthesis of a highly efficient, visible-light active and recyclable $TiO_2$-immobilized ruthenium polyazine complex for the C–H activation of tertiary amines to the corresponding α-aminonitriles.[11] However, limited accessibility and high cost are still the major drawbacks to be overcome by using low cost and non-toxic metals such as iron for photocatalytic applications.[12]

On the other hand, carbon dots have been identified as a novel photocatalytic support due to their non-toxic nature, easy synthesis, high surface area and ability to produce electron–hole pairs under visible light irradiation.[13] So far carbon quantum dots have widely been used as photocatalysts for the photodegradation of dyes under visible light irradiation. In this context, Zhang *et al.* reported the carbon quantum dot/$Ag_3PO_4$ complex as a photocatalyst for the photodecomposition of organic compounds (methyl orange) under visible light irradiation.[14] Liang *et al.* reported the synthesis and application of self-assembled Ag@AgCl QD sensitized $Bi_2WO_6$ for the photocatalytic degradation of Rhodamine B (RhB) dye under visible light irradiation.[15] Wei *et al.* prepared graphene quantum dots from chemically exfoliated multi-walled carbon nanotubes as an efficient photocatalyst for the degradation of organic dyes under visible-light irradiation.[16]

[a]*Institut d'Electronique, de Microélectronique et de Nanotechnologie (IEMN), UMR CNRS 8520, Université Lille 1, Avenue Poincaré, BP 60069 59652 Villeneuve d'Ascq, France. E-mail: rabah.boukherroub@univ-lille1.fr*
[b]*Département de Physique, Faculté des Sciences de Tunis, Université de Tunis-El Manar, 2092, Tunisia*
[c]*CSIR Indian Institute of Petroleum, Haridwar Road Mohkampur, Dehradun 248005, India. E-mail: suman@iip.res.in*
[d]*Academy of Scientific and Industrial Research (AcSIR), New Delhi, 110001, India*
[e]*State Key Laboratory of Luminescence and Applications, Changchun Institute of Optics, Fine Mechanics and Physics, Chinese Academy of Sciences, 3888 Dong Nanhu Road, Changchun 130033, China*
[f]*Centre des Recherches et des Technologies de l'Energie, B.P. 95 Hammam-Lif, 2050, Tunisia*

†Electronic supplementary information (ESI) available: Survey scan of XPS. See DOI: 10.1039/c6pp00203j

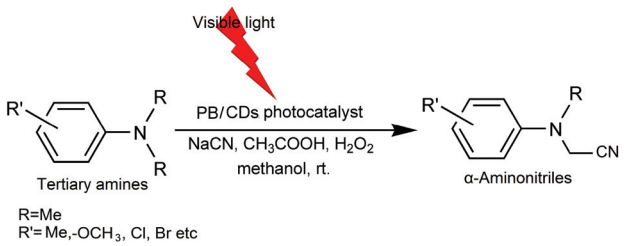


**Scheme 1** Photocatalytic C–H activation of tertiary amines using the PB/CD nanocomposite.

However, to the best of our knowledge, there is no literature report on the use of carbon quantum dots as a photocatalyst for C–H activation reactions. Accordingly, we report herein the successful synthesis of Prussian blue/carbon dot (PB/CD) nanocomposite and its application for C–H activation of tertiary amines under visible light irradiation at room temperature using NaCN/acetic acid as a cyanide source and hydrogen peroxide as an oxidant (Scheme 1).

## 2. Results and Discussion

### 2.1 Synthesis and characterization of PB/CD

Carbon dots were synthesized through alkaline hydrolysis of D-fructose at 50 °C as shown in Scheme 2. The desired Prussian blue was subsequently prepared in the presence of carbon quantum dots in a solution of $FeCl_2{\cdot}4H_2O$ and $K_3Fe(CN)_6$.[17]

The Raman spectrum of the PB/CD nanocomposite displayed two broad bands associated with the carbon dots. One is at ~1327 $cm^{-1}$ (D band) attributed to the $sp^3$-related defects; the other is at ~1583 $cm^{-1}$ (G band) assigned to the in-plane vibration of the $sp^2$ carbon.[18] In addition, three fingerprint vibration modes of PB appear at ~279, 506 and 2121 $cm^{-1}$,[19] confirming the formation of Prussian blue/carbon dot nanocomposite (Fig. 1).

Fig. 2 shows the FTIR spectra of PB, CDs and the PB/CD nanocomposite. The FTIR spectrum of PB depicts a characteristic band at 2091 $cm^{-1}$ due to the C≡N stretching of Fe–C≡N, and another strong/broad band at 3447 $cm^{-1}$ due to the –OH stretching of water (Fig. 2a). For CDs the absorption bands at 1632, 1386, 1120 $cm^{-1}$ were attributed to the bending vibration of water, the C=C stretching of polycyclic aromatic hydrocarbons in CDs and the C–O–C bending vibration of

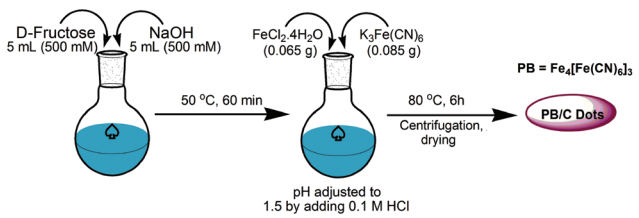


**Scheme 2** Synthesis of the PB/CD nanocomposite.

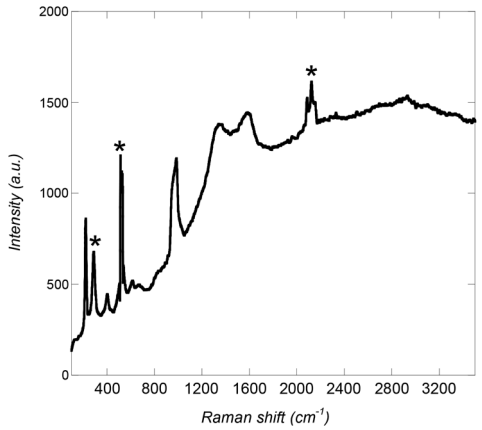


**Fig. 1** Raman spectrum of the PB/CD nanocomposite. * denotes the peaks due to PB.

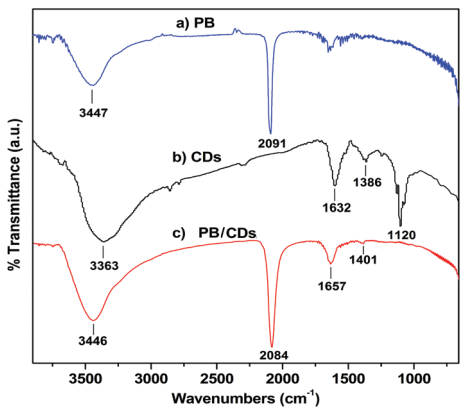


**Fig. 2** FTIR spectra of: (a) PB, (b) CDs, (c) PB/CD nanocomposite.

epoxide, respectively. The band at 3363 $cm^{-1}$ was assigned to the –OH stretch of adsorbed water and the –OH group present on carbon dots (Fig. 2b).[20,21] The FTIR spectrum of the PB/CD nanocomposite exhibits the characteristic Fe–C≡N band at 2084 $cm^{-1}$, typically used as a fingerprint for Prussian blue materials.[18] The stretching band at 1657 $cm^{-1}$ is assigned to the C=C stretching of polycyclic aromatic hydrocarbons in CDs. The broad band at 2900–3500 $cm^{-1}$ is ascribed to the stretching modes of the bonded (2973 $cm^{-1}$) and free (3446 $cm^{-1}$) –OH groups of the carbon dots and/or adsorbed water molecules (Fig. 2c).[22]

Fig. 3 shows the TEM images of the synthesized PB/CD nanocomposite. They mainly consist of some irregular nanoparticles in the range of ~30–100 nm. Some particles are spherical in morphology, while others are worm-like. The nanoparticles were not found to be stable under extended irradiation of electron beam during TEM observation. As shown in Fig. 3B and C, these particles decomposed into some much smaller ones (~3 nm) with an interplanar spacing of ~0.226 nm.

The survey spectrum of the PB/CD nanocomposite shows peaks at 284.4 eV ($C_{1s}$), 531.4 eV ($O_{1s}$), 398.1 eV ($N_{1s}$), and

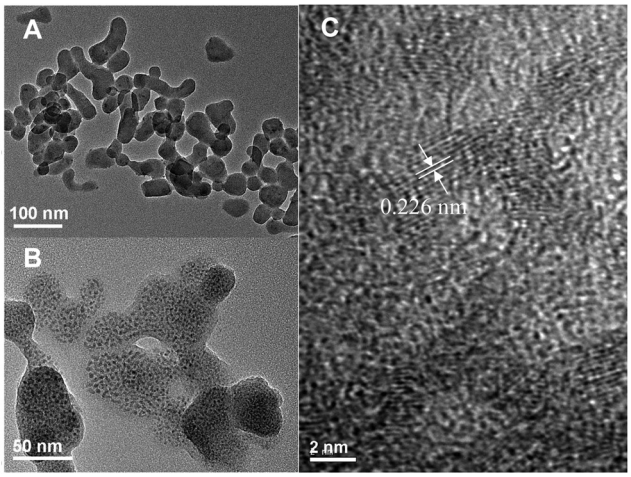


Fig. 3 TEM images of the PB/CD nanocomposite. The scale bars in A–C are 100, 50 and 2 nm, respectively.

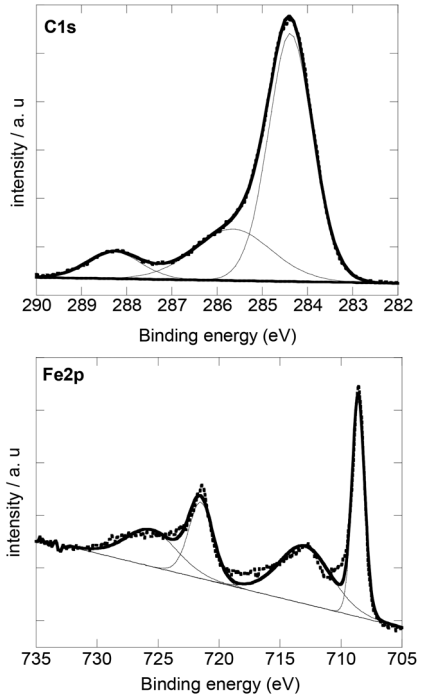


Fig. 4 C 1s and Fe 2p high-resolution XPS spectra of the PB/CD nanocomposite.

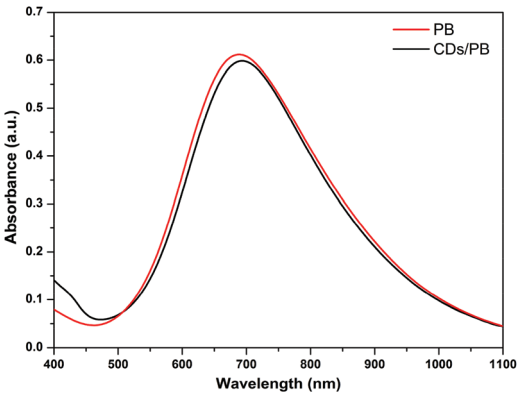


Fig. 5 UV-vis absorption spectra of (a) PB and (b) PB/CDs in the 400–1000 nm range.

708.4 eV ($Fe_{2p}$), in accordance with the chemical composition of the nanocomposite (Fig. S1†). The result confirmed the successful hybridization of PB nanoparticles with carbon dots. The high resolution C 1s XPS spectrum can be deconvoluted into three components with binding energies at about 284.4, 285.7 and 288.3 eV assigned to the $sp^2$-hybridized carbon, CN and C=O species, respectively.[23] The Fe 2p high resolution spectrum displays bands at 708.4, 712.8, 721.6 and 725.9 eV. The bands at 708.4 and 721.6 are assigned to $Fe^{2+}$ $2p_{3/2}$ and $2p_{1/2}$, respectively.[24] The peaks at 712.8 and 725.9 eV are due to $Fe^{3+}$ $2p_{3/2}$ and $2p_{1/2}$, respectively. These results are in good agreement with the formation of Prussian blue/carbon dot nanocomposite (Fig. 4).[25]

The nitrogen adsorption/desorption isotherm was used for the determination of the surface properties of the PB/CD nanocomposite (Fig. S2†). The adsorption/desorption isotherm of the PB/CD nanocomposite was found to be of type (I) with an H4 hysteresis loop. Furthermore, the BET surface area ($S_{BET}$), pore volume ($V_p$) and mean pore diameter of the PB/CD nanocomposite were determined to be 288.5 $m^2\ g^{-1}$, 0.18 $cm^3\ g^{-1}$ and 2.54 nm, respectively. The mean pore diameter between 2–50 nm, according to IUPAC recommendation, confirmed the mesoporosity of the material.[26]

The UV-visible absorption spectrum of PB in water shows a broad absorption band in the visible and near-infrared light range of 550 to 990 nm with a maximum ($\lambda_{max}$) at ~700 nm due to the charge transfer transition between Fe(II) and Fe(III) in PB (Fig. 5a). The profile of the absorption spectrum of the PB/CD nanocomposite follows closely that of PB in addition to a very slight decrease in absorbance, suggesting the presence of PB and low content of CDs in the nanocomposite (Fig. 5b).[27]

The fluorescence spectra of the PB/CD nanocomposite in water at different excitation wavelengths, recorded at room temperature, are displayed in Fig. 6. It shows that when the excitation wavelength increased from 320 to 420 nm, the corresponding emission peaks shifted from 455 to 510 nm, which illustrated the excitation-dependent emission. Furthermore, the most intense emission peak was observed at 475 nm for a 380 nm excitation wavelength. According to the quantum confinement effect, the band gap of CD nanoparticles as formed by the HOMO and LUMO is confined in size and strongly depends on the size of nanoparticles.[28] After excitation, the electrons are transferred to the LUMO and during relaxation, they return to the ground state with emission of light. Further change in the surface of CD nanoparticles through hybridization with PB is followed by a change in their optical properties (surface state defects).[29]

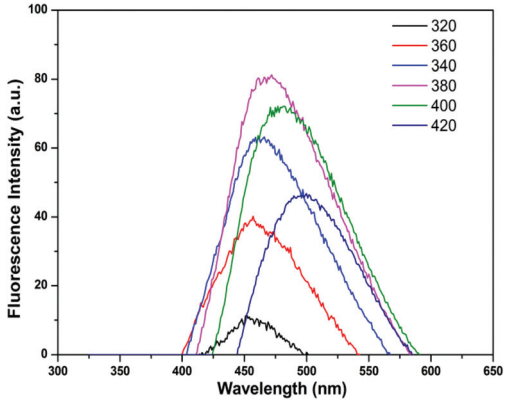


Fig. 6 Fluorescence spectra of the PB/CD nanocomposite in water at different excitation wavelengths recorded at room temperature.

### 2.2 Catalytic activity

The catalytic activity of the synthesized PB/CD nanocomposite towards the oxidative cyanation of tertiary amines to the corresponding α-aminonitriles was evaluated in the presence of NaCN/acetic acid as a source of cyanide, hydrogen peroxide ($H_2O_2$) as an oxidant and methanol as a solvent under visible irradiation, using a 20 W LED lamp under ambient conditions. *N*,*N*-Dimethylaniline was chosen as a model substrate for the optimization studies. In the absence of the photocatalyst, no product could be isolated even after 24 h of irradiation (Table 1, entry 1). Similarly, the presence of light was found to be vital and of prime importance for the reaction to proceed. In fact, in the absence of light irradiation, no reaction occurred using CDs, PB or the PB/CD composite (Table 1, entries 2, 4 and 6). Visible light was thus essential to drive the oxidative cyanation reaction. To confirm the superior activity of the PB/CD composite as compared to its individual components, we performed the reaction using CDs or PB under otherwise identical conditions. It was found that CDs alone provided a very small amount (8%) of the corresponding α-aminonitrile under visible light irradiation (Table 1, entry 3). This implies that the photo-generation of electron–hole pairs in the CDs could initiate the oxidative cyanation reaction, but the available redox sites at which electrons were efficiently transferred to the substrate are limited. Similarly, PB alone gave a poor yield of the desired product under the described reaction conditions (Table 1, entry 5). On the other hand, the PB/CD nanocomposite was found to be highly efficient and afforded nearly quantitative yield of the desired product within 8 h of irradiation (Table 1, entry 7). Furthermore, the presence of acetic acid was found to be essential and in its absence no reaction took place (Table 1, entry 8). The mixture of sodium cyanide/acetic acid produces HCN *in situ*, which was used as a source of nitrile for the reaction. Similarly, no reaction occurred in the absence of hydrogen peroxide (Table 1, entry 9).

In order to check the scope of the reaction, we performed the oxidative cyanation of various tertiary amines under the optimized conditions (Table 2). In all the cases, the conversion and selectivity of the desired product were determined by GC-MS. The identity of the products was confirmed by comparing the physical and spectral data with those of the authentic ones. Among various substituted *N*,*N*′-dimethyl anilines, those having substituents at the *para* position were more reactive (Table 2, entries 2, 4, 6 and 8) than those having *o*- and *m*-substituents (Table 2, entries 3, 5 and 7). Furthermore, the substrates having electron donating groups were found to be more active towards oxidative cyanation (Table 2, entries 2–4) than the substrates having an electron withdrawing group

Table 1 Effect of various parameters on oxidative cyanation of *N*,*N*′-dimethylaniline[a]

| Entry | Oxidant | Visible irradiation | Time (h) | Yield[b] (%) | TOF ($h^{-1}$) |
|---|---|---|---|---|---|
| 1 | $H_2O_2$ | Yes | 24 | — | — |
| 2 | $H_2O_2$ | No | 24 | — | — |
| 3 | $H_2O_2$ | Yes | 12 | 8 | 0.6 |
| 4 | $H_2O_2$ | No | 24 | — | — |
| 5 | $H_2O_2$ | Yes | 12 | 18 | 1.5 |
| 6 | $H_2O_2$ | No | 12 | — | — |
| 7 | $H_2O_2$ | Yes | 8 | 94 | 11.7 |
| 8 | $H_2O_2$ | Yes | 24 | —[c] | — |
| 9 | — | Yes | 12 | 6 | 0.5 |
| 10 | TBHP | Yes | 12 | 24 | 2.0 |
| 11 | $O_2$ | Yes | 12 | 15 | 1.2 |

[a] Reaction conditions: *N*,*N*′-dimethylaniline (1 mmol), photocatalyst (50 mg), NaCN (1.5 mmol), acetic acid (1 mL), $H_2O_2$ (2 mL), methanol (10 mL). [b] Isolated yield. [c] In the absence of acetic acid.

Table 2 PB/CD nanocomposite mediated oxidative cyanation of tertiary amines[a]

| Entry | Reactant | Product | Time (h) | Isolated yield[b] (%) | TOF ($h^{-1}$) |
|---|---|---|---|---|---|
| 1 |  |  | 8.0 | 94 | 11.7 |
| 2 | 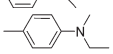 | 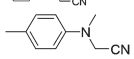 | 8.0 | 96 | 12.0 |
| 3 | 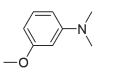 | 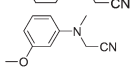 | 6.5 | 95 | 14.6 |
| 4 | 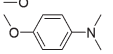 | 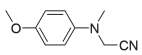 | 6.5 | 97 | 12.1 |
| 5 |  | 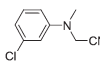 | 8.0 | 84 | 10.5 |
| 6 | 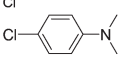 | 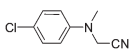 | 8.0 | 87 | 10.8 |
| 7 |  |  | 8.0 | 81 | 10.1 |
| 8 | 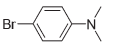 | 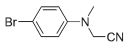 | 8.0 | 85 | 10.6 |
| 9 |  | 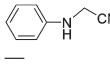 | 8.0 | 89 | 11.1 |
| 10 | $(n\text{-Bu})_3N$ | — | 24.0 | — | — |
| 11 |  |  | 12.0 | 12 | 1.0 |

[a] Reaction conditions: substrate (1 mmol), photocatalyst (50 mg), NaCN (1.5 mmol), acetic acid (1 mL), methanol (10 mL), $H_2O_2$ (2 mL). [b] Isolated yield.

(Table 2, entry 8). Secondary amines such as *N*-methylaniline also gave the corresponding cyano-product in good (89%) yield (Table 2, entry 6). Aliphatic tertiary amines like *n*-tributylamine did not give any product under the described reaction conditions (Table 2, entry 10). The reaction of tertiary amines having a benzyl group was found to be sluggish and provided very poor yield of the desired product (Table 2, entry 11).

Finally, we evaluated the recycling of the PB/CD photocatalyst which could be readily recovered from the reaction mixture after the completion of the reaction by centrifugation. The recovered photocatalyst was washed with methanol, dried and used as such for the subsequent experiments. The recovered catalyst was reused for the subsequent four runs and the results are summarized in Fig. 7. It was found that the recovered PB/CD photocatalyst showed almost equal activity and afforded 92, 90, 89 and 87% yield of the desired product.

In order to identify the photochemical species involved in oxidative cyanation of tertiary amines, we have carried out the reactions in the presence of the $^{\bullet}$OH radical and hole scavengers under otherwise identical reaction conditions.[30–32] Sodium bicarbonate was used as the $^{\bullet}$OH radical scavenger while EDTA·2Na was used as the hole scavenger. *N*,*N*′-Dimethylaniline was used as a model substrate and the yield of the product was monitored by withdrawing aliquots from the solution after every 2 h. It can be seen from Fig. 8 that upon addition of the $^{\bullet}$OH radical scavenger ($NaHCO_3$), the yield of α-aminonitriles decreased from 94% to 41% after 8 h, most likely due to the annihilation of the intermediate $^{\bullet}$OH radical produced from hydrogen peroxide. While upon addition of EDTA·2Na, the yield of the product slightly increased from 68% to 76% after 6 h and 94% to ~99% after 8 h, due to the positive hole scavenging by EDTA·2Na, which facilitates better charge separation on carbon dots.

On the basis of the existing literature,[33–35] we have proposed a plausible mechanism for the reaction (Scheme 3). In analogy to the existing reports, two important steps can be proposed for the photocatalytic oxidative cyanation of the tertiary amines. After absorption of visible light carbon dots are excited and generate electron–hole pairs and transfer electrons to PB. The iron either in Fe(II) or Fe(III) forms the oxo-iron(IV) intermediate in the presence of hydrogen peroxide.[36] This oxo-iron(IV) species abstracts a hydrogen from the α-carbon of the tertiary amine to give the cationic intermediate. Sodium cyanide in the presence of acetic acid provides *in situ* nitrile ions, which upon a nucleophilic attack gives the corresponding α-aminonitrile (Scheme 3).

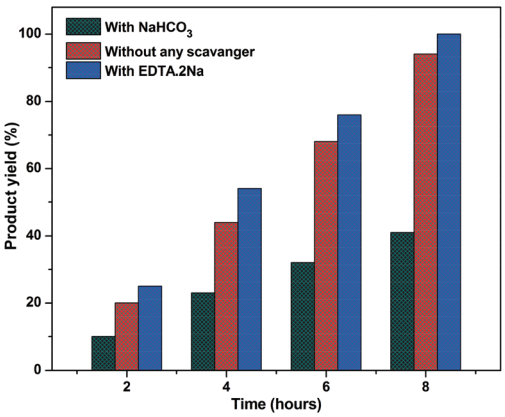


**Fig. 8** Yield of the cyanation product with or without addition of the $^{\bullet}$OH radical and hole scavengers.

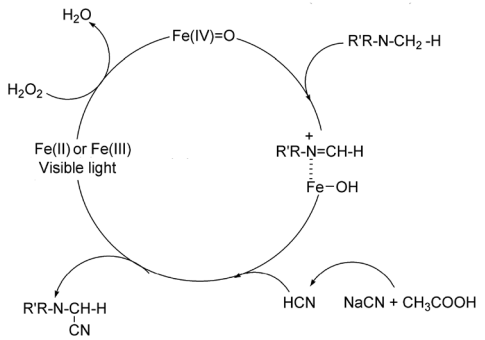


**Scheme 3** Plausible mechanism of the photocatalytic oxidative cyanation.

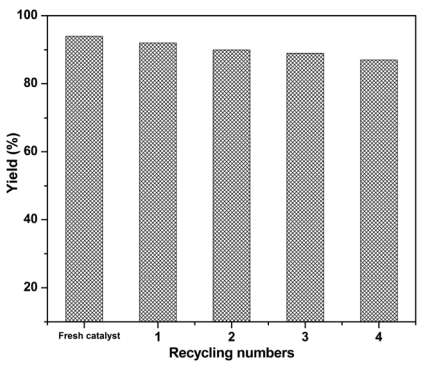


**Fig. 7** Recycling experiments using PB/CD as a photocatalyst.

## 3. Conclusion

In conclusion, we have synthesized a novel, non-noble metal based, visible light active PB/CD photocatalyst for the oxidative cyanation of aromatic tertiary amines to the corresponding α-aminonitriles by using house-hold LED visible light. After 8 h of irradiation, good to high yields of the products were obtained in the presence of $H_2O_2$ as an oxidant, NaCN/acetic acid as a source of nitrile and methanol as a solvent. The PB/CD photocatalyst was heterogeneous in nature, which could readily be recovered from the reaction mixture by centrifugation. The recovered catalyst exhibited consistent efficiency for the subsequent four runs without any significant loss in catalytic efficiency.

 

# 4. Experimental section

## 4.1 Materials

D-Fructose (≥99%), sodium hydroxide (≥97.0%), iron(II) chloride tetrahydrate, $Fe(II)Cl_2{\cdot}4H_2O$ (≥99.99%), potassium ferricyanide $K_3[Fe(CN)_6]$ (99%) and sodium cyanide (97%), were obtained from Sigma-Aldrich and used without further purification. Acetic acid and methanol (HPLC grade) were procured from Merck India Ltd and used as received.

## 4.2 Preparation of Prussian blue $Fe_4[Fe(CN)_6]_3$

To 20 mL water (pH adjusted to 1.5 with 0.1 M of HCl), 0.065 g of $FeCl_2{\cdot}4H_2O$ and 0.085 g of $K_3Fe(CN)_6$ were added. The color of the solution turned blue immediately. The resulting mixture was heated at 80 °C for 3 h. The final product was collected by centrifugation, washed several times with water and finally dried under vacuum overnight at 80 °C.

## 4.3 Preparation of the carbon dot/Prussian blue (PB/CD) nanocomposite[17]

An aqueous solution of carbon quantum dots (CDs) was prepared by mixing 5 mL of D-fructose (500 mM) and 5 mL of NaOH (500 mM), followed by heating the mixture at 50 °C for 60 min.

The above solution was adjusted to pH 1.5 by addition of 0.1 M HCl and then 0.065 g of $FeCl_2{\cdot}4H_2O$ and 0.085 g of $K_3Fe(CN)_6$ were added. The resulting mixture was heated at 80 °C for 6 h. The final product was collected by centrifugation, washed several times with water and finally dried overnight at 80 °C.

## 4.4 Characterization

TEM and high resolution TEM (HRTEM) images were acquired using an FEI Tecnai $G^2$-F20 transmission electron microscope operating at an acceleration voltage of 200 kV. The samples were drop-coated from ethanolic dispersion of PB/CD nanocomposite samples onto carbon-coated copper TEM grids and the solvent was evaporated under ambient conditions.

Micro-Raman measurements were carried out using a visible Labram HR spectrometer (Horiba Gr, France). The Raman backscattering was excited with a 532 nm excitation wavelength. The beam was focused on the sample surface through an optical objective (×100, 0.9 NA) with a lateral resolution (XY) of less than 1 μm. The obtained spectral resolution is better than 2 $cm^{-1}$.

X-ray photoelectron spectroscopy (XPS) measurements were performed with an ESCALAB 220 XL spectrometer from Vacuum Generators featuring a monochromatic Al Kα X-ray source (1486.6 eV) and a spherical energy analyzer operated in the CAE (constant analyzer energy) mode (CAE = 100 eV for survey spectra and CAE = 40 eV for high-resolution spectra), using the electromagnetic lens mode. The detection angle of the photoelectrons is 30°, as referenced to the sample surface. After subtraction of the Shirley-type background, the core-level spectra were decomposed into their components with mixed Gaussian–Lorentzian (30 : 70) shape lines using the CasaXPS software. Quantification calculations were performed using sensitivity factors supplied by PHI.

The samples were prepared by casting an ethanol suspension of the PB/CD nanocomposite on clean silicon wafers followed by drying in an oven at 60 °C to remove the solvent completely. The surface properties like BET surface area, pore size distribution *etc*. were estimated by the Brunauer–Emmett–Teller (BET) and Barrett–Joyner–Halenda (BJH) method with the help of a Micromeritics ASAP2010 instrument, using liquid nitrogen at 77 K.

Fluorescence spectra were measured on a Cary Eclipse spectrophotometer from Agilent Technologies. The absorption spectra of solutions in a quartz cuvette with an optical path of 10 mm were recorded using a Perkin Elmer Lambda UV/Vis 950 spectrophotometer in the wavelength range of 400–1100 nm. The samples were dispersed in water at a concentration of 50 μg $mL^{-1}$.

Fourier transform infrared (FTIR) spectra were recorded using a ThermoScientific FTIR instrument (Nicolet 8700) at a resolution of 4 $cm^{-1}$. The dried PB/CD sample (1 mg) was mixed with KBr powder (100 mg) in an agate mortar. The mixture was pressed into a pellet under a 10 ton load for 2–4 min, and the spectrum was recorded immediately. Sixteen accumulative scans were collected. The signal from a pure KBr pellet was subtracted as the background.

## 4.5 Experimental procedure for photocatalytic oxidative cyanation of tertiary amines

For the oxidative cyanation reaction, a 25 mL round bottomed flask was charged with tertiary amine (1 mmol), NaCN‡ (1.5 mmol), $H_2O_2$ (2 mL), methanol (10 mL), photocatalyst (50 mg) and acetic acid (1 mL). The reaction vessel was irradiated under visible light by using a 20 W LED lamp having an intensity at vessel of 75 W $m^{-2}$ at room temperature under continuous stirring. Progress of the reaction was monitored by TLC on a silica coated plate. After completion of the reaction, the photocatalyst was recovered by filtration. The obtained organic layer was washed with water and dried over anhydrous $Na_2SO_4$ followed by concentration in a rotary evaporator. The obtained crude product was purified by column chromatography over silica gel using ethyl acetate and hexane as the eluent to afford the corresponding α-aminonitriles. The identification and conversion of products was determined with GC-Mass and the obtained spectral data were matched with authentic samples in the GC-MS library.

# Acknowledgements

H. M., S. S. and R. B. acknowledge financial support from the Centre National de la Recherche Scientifique (CNRS), Lille1 University and Hauts-de-France region. PK and AK are thankful to the Director, CSIR-IIP for his kind permission to publish

‡Sodium cyanide is highly toxic and should be handled with care and gloves should be used during addition, separation, TLC and column chromatography.

these results. AK also acknowledges the CSIR, New Delhi, for their Research Fellowships.

## Notes and references

1 (*a*) L. Shi and W. Xia, *Chem. Soc. Rev.*, 2012, **41**, 7687–7697; (*b*) W.-P. To, Y. Liu, T.-C. Lau and C.-M. Che, *Chem. – Eur. J.*, 2013, **19**, 5654–5664.
2 (*a*) M. North, *Angew. Chem., Int. Ed.*, 2004, **43**, 4126–4128; (*b*) K. R. Campos, *Chem. Soc. Rev.*, 2007, **36**, 1069–1084; (*c*) S. Guo, B. Qian, Y. Xie, C. Xia and H. Huang, *Org. Lett.*, 2011, **13**, 522–525.
3 D. Enders and J. P. Shilvock, *Chem. Soc. Rev.*, 2000, **29**, 359–373.
4 S.-I. Murahashi, N. Komiya and H. Terai, *Angew. Chem., Int. Ed.*, 2005, **44**, 6931–6933.
5 K. Yamaguchi, Y. Wang and N. Mizuno, *ChemCatChem*, 2013, **5**, 2835–2838.
6 J. Peng, J. Zhao, Z. Hu, D. Liang, J. Huang and Q. Zhu, *Org. Lett.*, 2012, **14**, 4966–4969.
7 S. Singhal, S. L. Jain and B. Sain, *Chem. Commun.*, 2009, 2371–2372.
8 W. Han and A. R. Ofial, *Chem. Commun.*, 2009, 5024–5026.
9 Y. Zhang, H. Peng, M. Zhang, Y. Cheng and C. Zhu, *Chem. Commun.*, 2011, **47**, 2354–2356.
10 (*a*) M. Rueping, S. Zhu and R. M. Koenigs, *Chem. Commun.*, 2011, **47**, 12709–12711; (*b*) J. Lalevee, M. Peter, F. Dumur, D. Gigmes, N. Blanchard, M.-A. Tehfe, F. M. Savary and J. P. Fouassier, *Chem. – Eur. J.*, 2011, **17**, 15027–15031.
11 P. Kumar, S. Varma and S. L. Jain, *J. Mater. Chem. A*, 2014, **2**, 4514–4519.
12 (*a*) S. Singhal, S. L. Jain and B. Sain, *Adv. Synth. Catal.*, 2010, **252**, 1338–1344; (*b*) V. Panwar, P. Kumar, A. Bansal, S. S. Ray and S. L. Jain, *Appl. Catal., A*, 2015, **498**, 25–31; (*c*) S. Murata, K. Teramoto, M. Miura and M. Nomura, *Bull. Chem. Soc. Jpn.*, 1993, **66**, 1297–1298.
13 (*a*) K. A. S. Fernando, S. Sahu, Y. Liu, W. K. Lewis, E. A. Guliants, A. Jafariyan, P. Wang, C. E. Bunker and Y.-P. Sun, *ACS Appl. Mater. Interfaces*, 2015, **7**, 8363–8376; (*b*) L. Cao, S. Sahu, P. Anilkumar, C. E. Bunker, J. Xu, K. A. S. Fernando, P. Wang, E. A. Guliants, K. N. Tackett and Y.-P. Sun, *J. Am. Chem. Soc.*, 2011, **133**, 4754–4757; (*c*) P. G. Luo, S. Sahu, S.-T. Yang, S. K. Sonkar, J. Wang, H. Wang, G. E. LeCroy, L. Cao and Y.-P. Sun, *J. Mater. Chem. B*, 2013, **1**, 2116–2127.
14 H. Zhang, H. Huang, H. Ming, H. Li, L. Zhang, Y. Liu and Z. Kang, *J. Mater. Chem.*, 2012, **22**, 10501–10506.
15 Y. Liang, S. Lin, L. Liu, J. Hu and W. Cui, *Appl. Catal., B*, 2015, **164**, 192–203.
16 S. Wei, R. Zhang, Y. Liu, H. Ding and Y.-L. Zhang, *Catal. Commun.*, 2016, **74**, 104–109.
17 (*a*) Y. Li, X. Zhong, A. E. Rider, S. A. Furman and K. Ostrikov, *Green Chem.*, 2014, **16**, 2566–2570; (*b*) H. Bozetine, Q. Wang, A. Barras, M. Li, T. Hadjersi, S. Szunerits and R. Boukherroub, *J. Colloid Interface Sci.*, 2016, **465**, 286–294.
18 (*a*) S. N. Baker and G. A. Baker, *Angew. Chem., Int. Ed.*, 2010, **49**, 6726–6744; (*b*) X. Zhang, H. Ming, R. Liu, X. Han, Z. Kang, Y. Liu and Y. Zhang, *Mater. Res. Bull.*, 2013, **48**, 790–794.
19 (*a*) A. M. Farah, N. D. Shooto, F. T. Thema, J. S. Modise and E. D. Dikio, *Int. J. Electrochem. Sci.*, 2012, **7**, 4302–4313; (*b*) S.-C. Jang, Y. Haldorai, G.-W. Lee, S.-K. Hwang, Y.-K. Han, C. Roh and Y. S. Huh, *Sci. Rep.*, 2015, **5**, 17510.
20 P. Kumar, H. P. Mungse, S. Cordier, R. Boukherroub, O. P. Khatri and S. L. Jain, *Carbon*, 2015, **94**, 91–100.
21 X.-Q. Zhang, S.-W. Gong, Y. Zhang, T. Yang, C.-Y. Wang and N. Gu, *J. Mater. Chem.*, 2010, **20**, 5110–5116.
22 M. Melucci, M. Durso, M. Zambianchi, E. Treossi, Z.-Y. Xia, I. Manet, G. Giambastiani, L. Ortolani, V. Morandi, F. De Angelis and V. Palermo, *J. Mater. Chem.*, 2012, **22**, 18237–18243.
23 (*a*) H. Wu, G. Gao, X. Zhou, Y. Zhang and S. Guo, *CrystEngComm*, 2012, **14**, 499–504; (*b*) P. Kumar, H. P. Mungse, O. P. Khatri and S. L. Jain, *RSC Adv.*, 2015, **5**, 54929–54935; (*c*) A. Kumar, P. Kumar, C. Joshi, S. Ponnada, A. K. Pathak, A. Ali, B. Sreedhar and S. L. Jain, *Green Chem.*, 2016, **18**, 2514–2521.
24 (*a*) Z. Geng, Y. Lin, X. Yu, Q. Shen, L. Ma, Z. Li, N. Pan and X. Wang, *J. Mater. Chem.*, 2012, **22**, 3527–3535; (*b*) S. Zhang, W. Li, B. Tan, S. Chou, Z. Li and S. Dou, *J. Mater. Chem. A*, 2015, **3**, 4793–4798.
25 L. Chen, X. Wang, X. Zhang and H. Zhang, *J. Mater. Chem.*, 2012, **22**, 22090–22096.
26 J. Rouquerol, D. Avnir, C. W. Fairbridge, D. H. Everett, J. M. Haynes, N. Pernicone, J. D. F. Ramsay, K. S. W. Sing and K. K. Unger, *Pure Appl. Chem.*, 1994, **66**, 1739–1758.
27 Y.-P. Sun, B. Zhou, Y. Lin, W. Wang, K. A. S. Fernando, P. Pathak, M. J. Meziani, B. A. Harruff, X. Wang, H. Wang, P. G. Luo, H. Yang, M. E. Kose, B. Chen, L. M. Veca and S.-Y. Xie, *J. Am. Chem. Soc.*, 2006, **128**, 7756–7757.
28 H. Shi, J. Wei, L. Qiang, X. Chen and X. Meng, *J. Biomed. Nanotechnol.*, 2014, **10**, 2677–2699.
29 S. Zhu, Y. Song, X. Zhao, J. Shao, J. Zhang and B. Yang, *Nano Res.*, 2015, **8**, 355–381.
30 S. Lin, L. Liu, J. Hu, Y. Liang and W. Cui, *Appl. Surf. Sci.*, 2015, **324**, 20–29.
31 Y. Liang, S. Lin, L. Liu, J. Hu and W. Cui, *Appl. Catal., B*, 2015, **164**, 192–203.
32 W. Cui, H. Wang, L. Liu, Y. Liang and J. G. McEvoy, *Appl. Surf. Sci.*, 2013, **283**, 820–827.
33 (*a*) S.-I. Murahashi, T. Nakae, H. Terai and N. Komiya, *J. Am. Chem. Soc.*, 2008, **130**, 11005–11012; (*b*) S.-I. Murahashi, N. Komiya, H. Terai and T. Nakae, *J. Am. Chem. Soc.*, 2003, **125**, 15312–15313.
34 S.-I. Murahashi and D. Zhang, *Chem. Soc. Rev.*, 2008, **37**, 1490–1501.
35 Y. Zhang, H. Peng, M. Zhang, Y. Cheng and C. Zhu, *Chem. Commun.*, 2011, **47**, 2354–2356.
36 C. L. Sun, B. J. Li and Z.-J. Shi, *Chem. Rev.*, 2011, **111**, 1293–1314.

 